Journal of Materials Research and Technology 28 (2024) 3155–3165

Contents lists available at ScienceDirect

Journal of Materials Research and Technology

journal homepage: www.elsevier.com/locate/jmrt

Low cycle fatigue and creep-fatigue interaction behavior of 2.25CrMoV steel at high temperature

Furen Chen [a], Wei Zhang [a,*], Kaihao Zhang [a], Qiaofa Yang [a], Xiaoxiao Wang [b], Changyu Zhou [a,**]

[a] School of Mechanical and Power Engineering, Nanjing Tech University, Nanjing, 211816, China
[b] Department of Mechanical and Aerospace Engineering, University of Strathclyde, Glasgow, G1 1XJ, UK

ARTICLE INFO

Keywords:
2.25CrMoV steel
Low cycle fatigue
Creep-fatigue interaction
Microstructure
Fatigue life prediction

ABSTRACT

This paper presents a comprehensive investigation into the low cycle fatigue (LCF) and creep-fatigue interaction (CFI) behavior of 2.25CrMoV steel at an elevated temperature of 455 °C. The LCF tests are conducted using a triangular waveform with varying strain amplitudes ranging from 0.4 % to 0.7 %. Furthermore, the CFI tests are conducted using a trapezoidal waveform with different hold times and hold directions. To gain further insights, the microstructure and fracture behavior of the steel are characterized using optical, scanning, and transmission electron microscopy techniques. The results reveal that the softening behavior and fatigue life degradation of the steel are dependent on the applied strain amplitude, hold time, and hold direction. Higher strain amplitudes in the LCF tests lead to an increased number of crack initiation sources. During the CFI tests, fatigue fracture is identified as the primary failure mechanism under tensile hold conditions, and an increase in hold time promotes crack propagation. The interaction between fatigue and creep is found to be more significant in compressive hold and tensile compressive combination hold conditions. Microstructure analysis demonstrates that the lath structure recovers during cyclic loading, resulting in cyclic softening. Finally, a modified energy-based model is proposed to distinguish the different roles of tensile energy and compressive energy in the fatigue process. The proposed model accurately predicts the fatigue life of the 2.25CrMoV steel, as demonstrated by the good agreement between the experimental and predicted results.

1. Introduction

With the rapid development of petrochemical industry, hydrogenation equipment is now required to operate at higher temperatures and pressures [1–3]. The traditional 2.25CrMo steel, which has been commonly used in hydrogenation equipment, is no longer suitable for new processes [4,5]. However, the carbides formed by the addition of V element and carbon element in the steel can significantly enhance its high temperature performance [6–8]. Therefore, V-modified steels, such as 2.25CrMoV steel, have been introduced as replacements for traditional 2.25CrMo steel in the manufacturing of hydrogenation equipment. During operational conditions, the high-temperature components within the hydrogenation reactor are often subjected to cyclic loading, including startup and shutdown periods [9–11]. Additionally, in high-temperature and high-pressure working environments, creep damage inevitably occurs [12–14]. Consequently, these components always experience damage caused by low cycle fatigue (LCF) and creep fatigue interaction (CFI) [15–17].

In the past decades, extensive studies have been conducted on the LCF and CFI of various materials, including 304SS and 316SS [18–21], 2.25Cr1Mo steel [22,23], and 9Cr–1Mo steel [24], among others. In LCF, materials typically exhibit cyclic hardening or softening behavior. For instance, Paul et al. [25] investigated LCF behavior of 304LN SS and found that it displayed cyclic hardening characteristics due to dislocation multiplication and tangle during fatigue, enhancing its resistance to deformation. Tian et al. [26] observed that 2.25CrMoV steel undergoes dislocation rearrangement during cyclic loading, reducing its ability to resist cyclic deformation and leading to local stress concentration. These stress concentration areas further promote local deformation and microcrack propagation of the material, resulting in significant cyclic softening. Studies on EUROFER97 by Zahran et al. [27–29] revealed pronounced cyclic softening, particularly at higher temperatures and strain amplitudes. The elevated temperature and high strain amplitude cause increased microstructural instability, leading to cyclic softening

* Corresponding author.
** Corresponding author.
E-mail addresses: zhang_wei@njtech.edu.cn (W. Zhang), changyu_zhou@163.com (C. Zhou).

https://doi.org/10.1016/j.jmrt.2023.12.233
Received 12 October 2023; Received in revised form 17 December 2023; Accepted 24 December 2023
Available online 27 December 2023

[30]. During cyclic loading, a decrease in dislocation density within the lath structure and recovery of low-angle grain boundaries were also observed [31,32]. These characteristics contribute to cyclic softening, particularly at high temperatures, accompanied by enhanced localized oxidation at the surface slip bands [33]. On the other hand, CFI tests usually involve introducing hold times based on the LCF tests, and the effects of hold time and direction on material deformation behavior have been investigated. Srinivasan et al. [18] and Mohammad et al. [20] studied the CFI deformation of 316L(N) SS and found that fatigue life decreased with increasing hold time. Chen et al. [34,35] studied the CFI behavior of 2.25Cr1Mo(V) steel and observed stress relaxation during hold time, which could influence fatigue life. In comparison with tensile hold, compressive hold has a relatively minor impact on fatigue life, and Goswami's research even indicated that compressive hold was beneficial for fatigue life at higher strain ranges [36]. Rho's study on Nb-A286 alloy also obtained similar results, showing that compressive hold can heal creep voids, reducing interaction with grain boundary precipitates and resulting in less damage [37]. For 2.25Cr1Mo steel, 9Cr–1Mo steel, and RAFM steel, previous studies have shown that compressive hold results in a shorter life compared to tensile hold [22,24,38,39]. This trend can be attributed to the generation of mean tensile stress during compressive hold, which promotes creep damage. Additionally, the oxidation-fatigue interaction plays a role. Shankar's research on RAFM steel indicated that tensile hold tends to form thicker oxide films, passivating cracks surfaces. Conversely, compressive hold breaks down the oxide film, increase oxidation, promote crack growth, and reduce life [38]. Although a large amount of CFI of different materials have been reported [40–45], related LCF and CFI data on 2.25CrMoV are still limited. Therefore, studying LCF and CFI of 2.25CrMoV is crucial for gaining a comprehensive understanding of material properties and life prediction of this alloy.

In this work, a series LCF and CFI tests are conducted on 2.25CrMoV steel. The deformation behaviors, including cyclic stress response, cyclic stress-strain hysteresis loop, and stress relaxation, are discussed. Then, the microstructure characterization and fracture morphology are presented. The detailed relationship between cyclic deformation, microstructure evolution, and fracture morphology of 2.25CrMoV steel under LCF and CFI conditions is further discussed. Finally, a modified energy-based life prediction model for 2.25CrMoV steel is proposed, which distinguishes the roles of tensile and compressive energy, and its accuracy is verified through the test data.

2. Experimental procedures

The material under investigation in this study is a 2.25CrMoV steel, and its chemical composition is presented in Table 1. According to ASTM E606 [46], cylindrical specimens were fabricated, featuring a gauge length of 15 mm and a diameter of 6 mm (Fig. 1).

Both LCF and CFI tests were carried out under a strain rate of $1\times 10^{-3}s^{-1}$ and a temperature of 455 $^{\circ}C$. For the LCF tests, different strain amplitudes of 0.4 %, 0.5 %, 0.6 %, and 0.7 % were applied. Shankar et al. [38] suggested that the CFI tests introduce hold time at lower strain amplitudes to approach the real situation. Accordingly, a strain amplitude of 0.4 % was chosen for the CFI tests, with tensile hold times ranging from 5 s to 180 s. Additionally, different hold directions were applied at hold times of 10 s and 60 s, as outlined in Table 2. Furthermore, CFI tests with varying strain amplitudes were conducted under a hold time of 60 s to examine the influence of strain amplitudes. The loading waveforms for both the LCF and CFI tests are presented in Fig. 2. The fatigue life (N_f) was defined as the point at which a 10 % decrease in peak tensile stress occurred during the stable stage of the test.

After LCF and CFI failure, the microstructure of the specimens was characterized to unravel the underlying microstructural damage mechanisms and fracture features. For the fractured specimens, a two-fold approach was employed. Firstly, one portion was examined using a scanning electron microscope (SEM, JSM-6360LV) to provide a macroscopic view of the fracture surface. Secondly, the remaining section was studied using a transmission electron microscope (TEM, JEOL-2100F) to investigate the microstructure at a finer scale. This section was carefully cut near the fracture surface to obtain thin plates with a thickness of 0.5 mm. These plates were subsequently polished and stamped into slices measuring 80 μm in thickness and 3 mm in diameter.

3. Experimental results and discussion

3.1. Cyclic stress response

The cyclic stress response under various loading conditions is depicted in Fig. 3. The cyclic softening curve exhibits three distinct stages: rapid softening, stable, and final failure stage. During the final failure stage, macro cracks become apparent on the test specimen, leading to a rapid decrease in peak tensile stress as a result of crack propagation [47]. Under LCF condition (Fig. 3(a)), as the strain amplitude increases, the softening characteristics of the material become more pronounced. Introducing a hold time does not alter the cyclic softening behavior but accelerates the softening process (Fig. 3(b) and (c)). This accelerated softening can be attributed to the creep strain generated during the hold time, which affects the internal microstructure of the material and reduces its ability to resist cyclic deformation [48]. Regarding the cyclic softening curves with different hold directions (Fig. 3(d)), the combination of tensile and compressive hold exhibits the most pronounced cyclic softening behavior. Conversely, the difference between shorter hold times and the sole application of either tensile or compressive hold is not significant.

The softening ratio (S) was also adopted in the present study to further elucidate the influences of hold time and hold direction, which is expressed as the following equation [49]:

$$S = \left(\sigma_a^1 - \sigma_a^{half}\right) / \sigma_a^1 \tag{1}$$

where σ_a^1 and σ_a^{half} are the stress amplitudes at the first cycle and half-life cycle. The softening ratio (S) exhibits an increasing trend with the increase of strain amplitude, as illustrated in Fig. 4(a). Upon introducing a hold time (Fig. 4(b)), the softening ratio demonstrates an overall increase, although the extent of this increase varies. Moreover, as the hold time is prolonged, the softening ratio continues to rise, with different hold directions yielding distinct effects. Notably, compressive hold generates the lowest softening ratio, while the combination of tensile and compressive hold yields the highest ratio. During cyclic loading, the dislocations within the material undergo rearrangement, reducing its ability to resist deformation [24]. This, in turn, promotes cyclic softening and leads to the occurrence of local stress concentrations. These localized stress concentration areas further facilitate local deformation and microcrack propagation within the material [26].

The evaluation of mean stress is another crucial indicator of cyclic deformation behavior under both LCF and CFI loading conditions. Fig. 5 presents the evolution of mean stress under different loading conditions. In the LCF tests, an asymmetric behavior was observed, with the mean stress exhibiting a compressive trend. Fig. 5(a) illustrates that the most

Table 1
Chemical compositions of 2.25Cr1MoV steel (Wt.%).

C	Si	Mn	P	S	Cr	Mo	Ni	V	Cu	Al
0.15	0.07	0.56	0.006	0.002	2.44	0.96	0.12	0.263	0.03	0.011

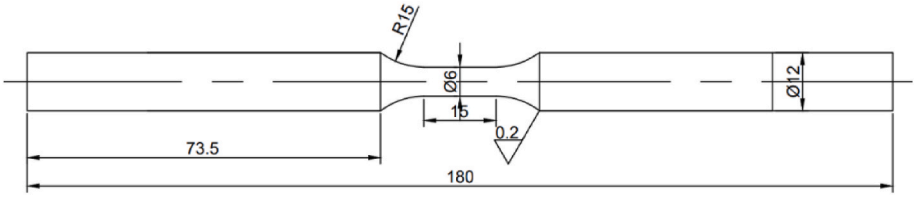

Fig. 1. Schematic illustration of the specimen (units: mm).

Table 2
Detailed test conditions for 2.25CrMoV steel.

Test No.	Temperature (°C)	strain amplitude (%)	Hold time (s)	strain rate (s^{-1})	Fatigue life (*N*)
IF04455	455	±0.4	/	1×10^{-3}	2725
IF05455	455	±0.5	/	1×10^{-3}	1184
IF06455	455	±0.6	/	1×10^{-3}	811
IF07455	455	±0.7	/	1×10^{-3}	591
IF04455TH5	455	±0.4	5	1×10^{-3}	2021
IF04455TH10	455	±0.4	10	1×10^{-3}	1839
IF04455TH30	455	±0.4	30	1×10^{-3}	1764
IF04455TH60	455	±0.4	60	1×10^{-3}	1556
IF04455TH180	455	±0.4	180	1×10^{-3}	1443
IF04455CH10	455	±0.4	10	1×10^{-3}	1720
IF04455TCH10	455	±0.4	10	1×10^{-3}	1690
IF04455CH60	455	±0.4	60	1×10^{-3}	1536
IF04455TCH60	455	±0.4	60	1×10^{-3}	1126
IF05455TH60	455	±0.5	60	1×10^{-3}	960
IF06455TH60	455	±0.6	60	1×10^{-3}	617
IF07455TH60	455	±0.7	60	1×10^{-3}	507

pronounced asymmetric behavior occurs at a strain amplitude of 0.4 %, and this asymmetry weakens as the strain amplitude increases. During the third stage of cyclic softening, as the initiation and propagation of macroscopic crack, the mean stress experiences a rapid increase until failure. Upon introducing a hold time (Fig. 5(b) and (c)), the asymmetric behavior and compressive mean stress are enhanced, while the overall trend of mean stress evolution remains unchanged. Furthermore, with the increase of time, the asymmetric behavior become increasingly evident. The mean stress generated by different hold directions also exhibits variations, as shown in Fig. 5(d). Compressive hold results in a mean tensile stress, whereas the combination of tensile and compressive hold ultimately leads to a mean compressive stress. Both of these stresses increase with longer hold times. Notably, some investigations [42,50] have indicated that the introduction of hold time can accelerate the evolution of the material's microstructure.

Fig. 6 illustrates the fatigue life under different loading conditions. Both LCF and CFI loadings (Fig. 6(a)) exhibit a notable reduction in fatigue life with increasing strain amplitude. Additionally, the introduction of hold time exacerbates the creep damage, leading to further reduction in fatigue life. Fig. 6(b) provides a comparative analysis of the effects of different hold times and hold directions on fatigue life. It is evident that the effect of hold time on fatigue life becomes more pronounced with increasing hold time. As the hold time increases, the fatigue life continuously decreases. Moreover, the fatigue life under compressive hold is shorter compared to that under tensile hold. Notably, when a combination of tensile and compressive hold is applied, the fatigue life experiences an even greater reduction. This observation may be attributed to oxidation and microstructural changes, which contribute to the decreased fatigue life.

3.2. Cyclic stress-strain hysteresis loop

Fig. 7(a) and (b) present the influence of strain amplitude and the introduction of hold time on the half-life stress-strain hysteresis loop in LCF and CFI tests, respectively. As the strain amplitude increases (Fig. 7 (a)), the peak tensile stress increases continuously, accompanied by an increase in the width of the hysteresis loop. Upon introducing the hold time (Fig. 7(b)), obvious stress relaxation occurs in the maximum strain. The enclosed area of the hysteresis loop represents the plastic strain energy generated by the material during a single loading cycle. A larger area indicates greater plastic deformation of the material and higher consumption of plastic strain energy. The variation of stress-strain hysteresis loops with different hold times is relatively insignificant, as depicted in Fig. 7(c). When the hold time is less than 60 s, the hysteresis loops remain largely consistent. However, with an increase in hold time to 180 s, the tensile peak stress exhibits a evident decrease. In Fig. 7(d) and (e), the stress-strain hysteresis loops under different hold directions are compared. Comparing the results at 10 s and 60 s, it is evident that the peak tensile stress under compressive hold is slightly higher than that under other conditions. Furthermore, the hysteresis loop width is greater for the tensile hold and the combination of tensile and compressive hold, in comparison to the compressive hold condition.

Fig. 8 provides a comparison of the plastic strain energy under different loading conditions. As the strain amplitude increases (Fig. 8 (a)), the plastic strain energy during the half-life period also increases, resulting in greater damage and a reduction in fatigue life. Furthermore, comparing the plastic strain energy of different hold times (Fig. 8(b)), it is evident that the plastic strain energy increases with longer hold times. Regarding different hold directions, the compressive hold exhibits the lowest amount of plastic strain energy, while the combination of tensile and compressive hold demonstrates the highest amount. Fig. 8(c) and (d) respectively show the proportion of tensile plastic strain energy and compressive plastic strain energy under different strain amplitudes and tensile hold times of the half-life cycle. It is observed that the compressive plastic strain energy is slightly higher than the tensile part, indicating that compressive plastic strain energy contributes more significantly to material damage. This observation should be taken into account when predicting the material's fatigue life.

3.3. Evolution of stress relaxation

In the CFI tests, stress relaxation occurs during the hold time (Fig. 7), leading to an increase in creep strain and creep damage. Fig. 9 depicts the relationship between relaxed stress and time during the half-life cycle under different loading conditions. It is observed that at the onset of the hold time, there is a rapid decrease in stress. At different strain amplitudes, as shown in Fig. 9(a), the stress experiences an initial rapid decline within the first 10 s, followed by a stabilization stage with

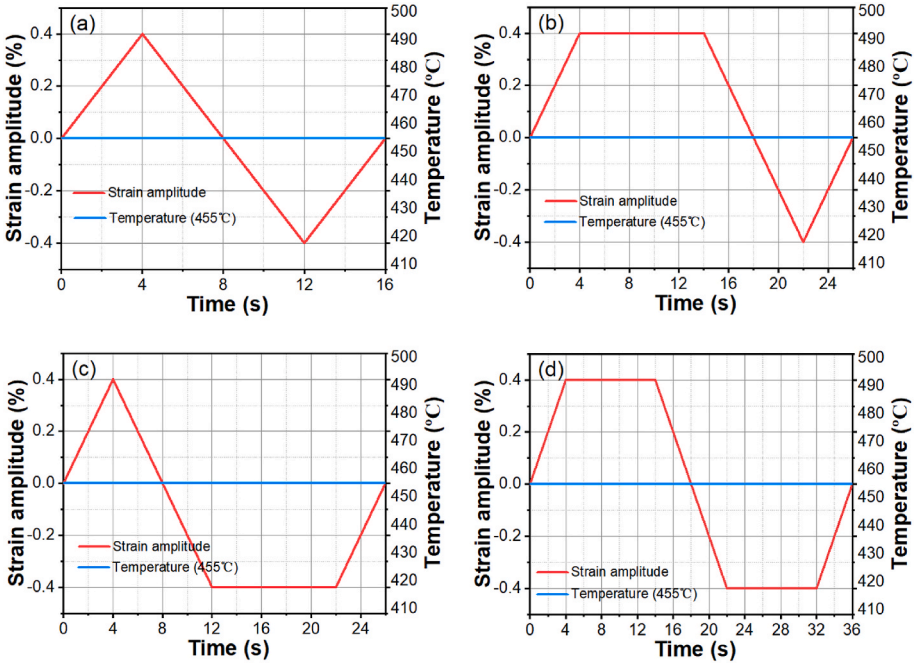

Fig. 2. Loading waveform: (a) LCF, (b) CFI with tensile strain hold (TH), (c) CFI with compressive strain hold (CH), and (d) CFI with balanced strain hold (TCH).

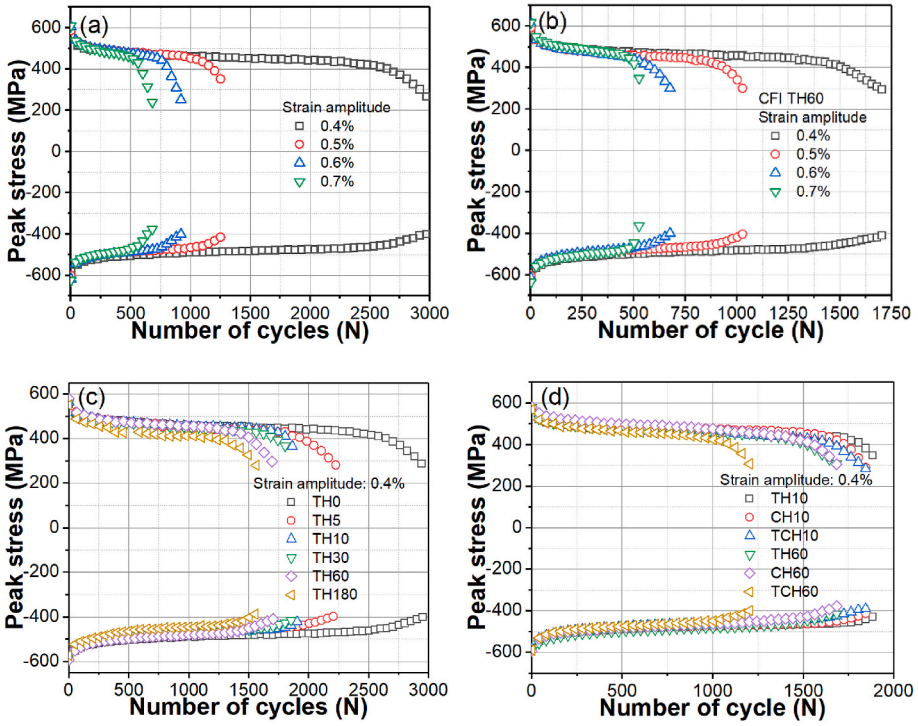

Fig. 3. Cyclic stress response: (a) LCF, (b) tensile hold at different strain amplitudes, (c) tensile hold with different hold times, and (d) different directions hold.

a slower rate of stress decrease, ultimately reaching a steady state. During this stable state, the stress relaxation curves exhibit parallel behavior regardless of the strain amplitude, indicating that the stress relaxation rate remains unaffected by the strain amplitude. As the hold time increases (Fig. 9(b)), the stress evolution curves nearly overlap within 60 s. However, when the hold time extends to 180 s, a significant increase in stress relaxation is observed. Fig. 9(c) compares the effects of different hold directions on stress relaxation. The stress evolution curves for both tensile hold and compressive hold are parallel, with similar stress relaxation rates and amounts during the hold time. However, for the combination of tensile and compressive hold, the stress relaxation amount increases due to the longer hold time.

The stress relaxation amount per cycle is also a important parameter that describes the CFI behavior of materials. Fig. 10 depicts the evolution of the stress relaxation amount under different strain amplitudes, hold times, and directions. Evidently, stress relaxation amount also exhibits three distinct stages: rapid softening, stable and final failure. The increase in strain amplitude has little impact on the stress relaxation

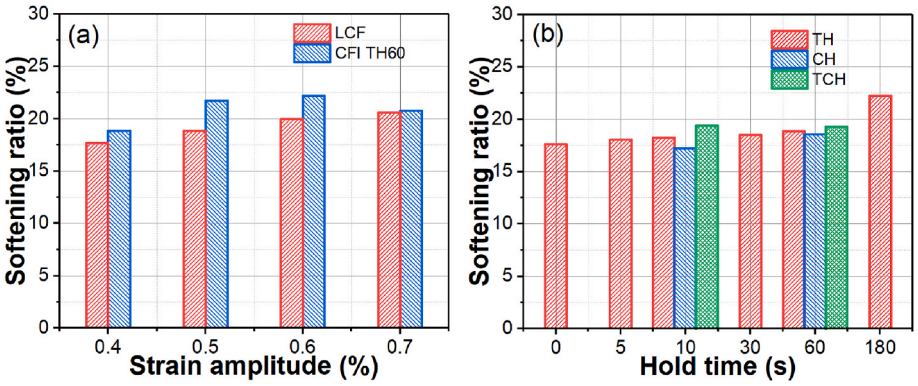

Fig. 4. Softening ratio: (a) LCF and CFI at different strain amplitude and (b) CFI with different hold times and directions.

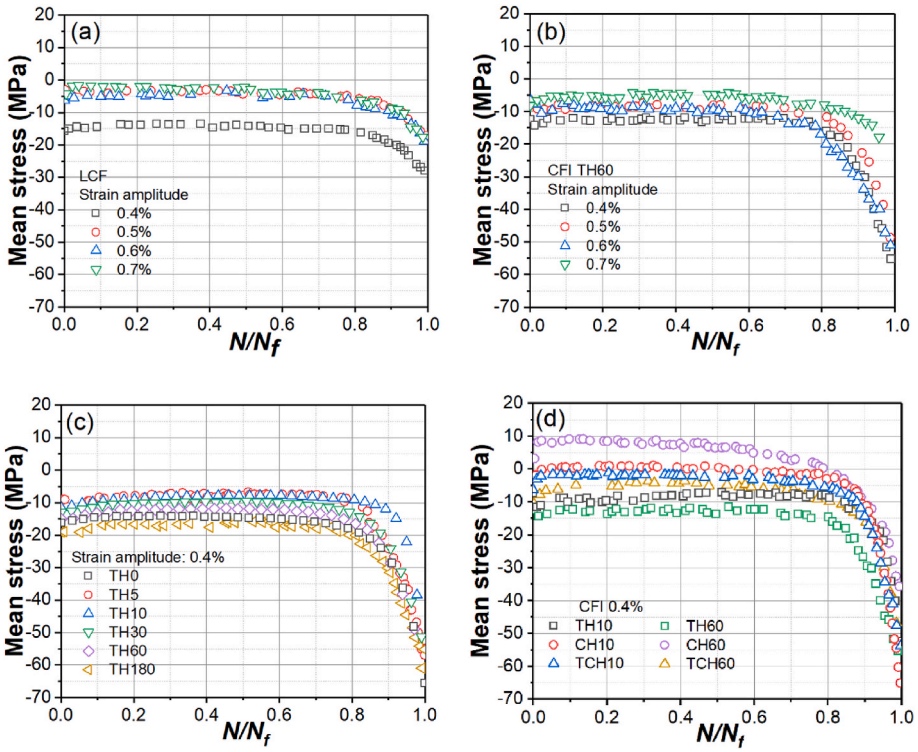

Fig. 5. The evolution of mean stress under different loading conditions: (a) LCF, (b) tensile hold at different strain amplitudes, (c) tensile hold with different hold times, and (d) different directions hold.

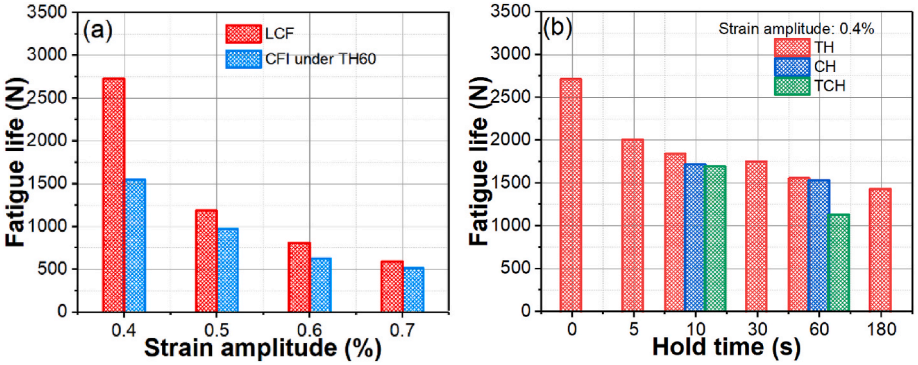

Fig. 6. Fatigue life under different loading conditions: (a) LCF and CFI at different strain amplitudes, and (b) CFI with different hold times and directions.

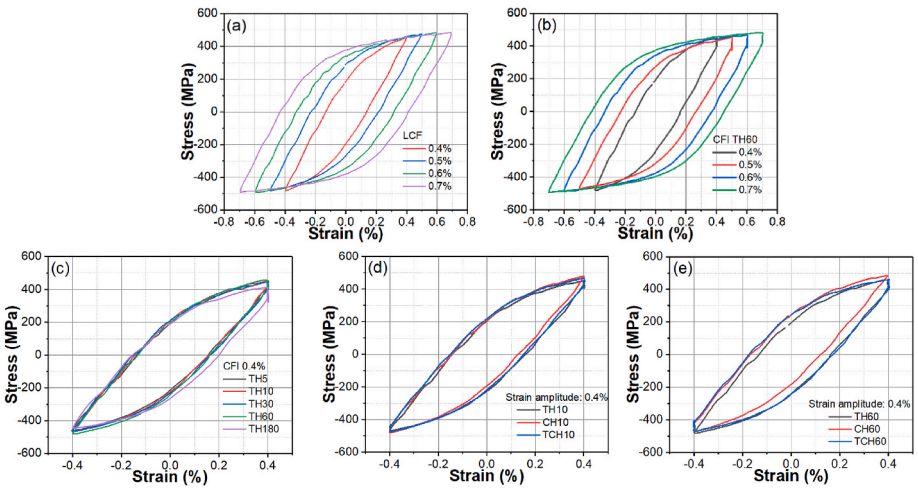

Fig. 7. Cyclic stress-strain hysteresis loop under different conditions: (a) LCF, (b) tensile hold at different strain amplitude, (c) tensile hold with different hold times, (d) and (e) different directions hold with 10 s and 60 s.

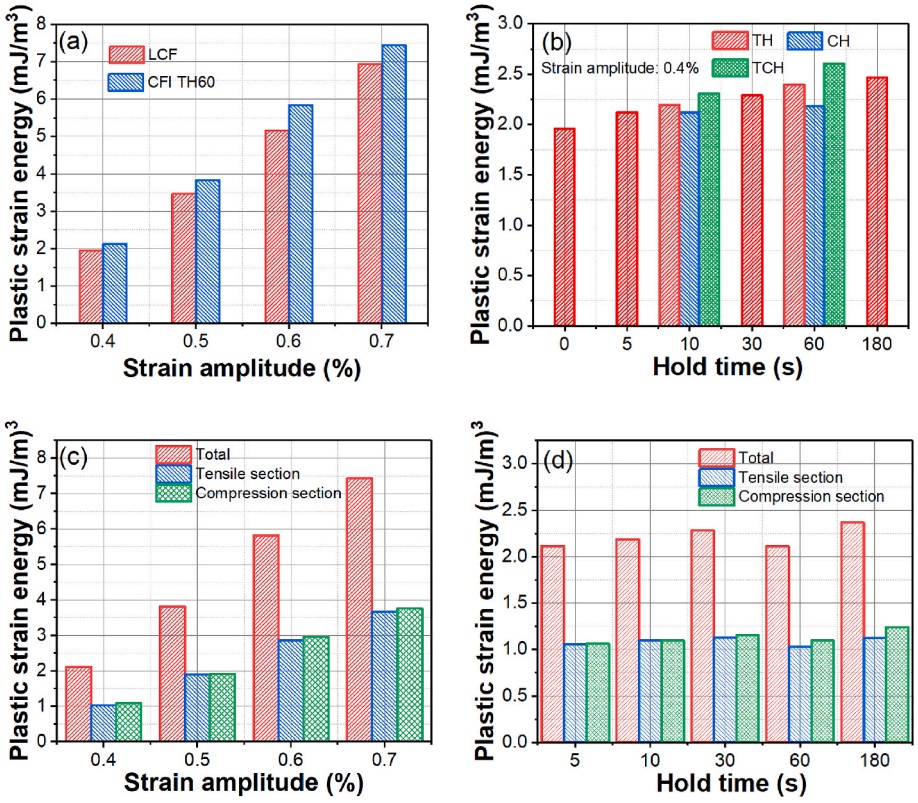

Fig. 8. Plastic strain energy under different loading conditions: (a) LCF and CFI under different strain amplitudes, (b) different hold times and directions, (c) and (d) plastic strain energy at different directions.

amount, as shown in Fig. 10(a). However, as depicted in Fig. 10(b), the stress relaxation amount increases with longer hold times. It is worth mentioning that stress relaxation amount reaches a stable state at a hold time of 60 s, as evidenced by achieving the same value of relaxation stress as the 30 s hold time. However, when the hold time is sufficiently long, such as 180 s, a significant increase in stress relaxation amount is observed again. This can be attributed to the long-term CFI test, which results in microstructure evolution and severe oxidation [48]. The influence of different hold directions on stress relaxation is also relatively small, as shown in Fig. 10(c). The stress relaxation curves for both tensile hold and compressive hold align closely.

3.4. Fractographic observation

Fig. 11 presents the fractographs of LCF specimens at different magnifications, with Fig. 11(c) and (d) providing locally magnified views. The yellow arrows indicate the location of crack initiation. It is evident that higher strain amplitudes result in a greater number of crack initiation sites (Fig. 11(a) and (b)). The matrix and surface of the material generate more slip bands to adapt to high strain amplitude, and the slip bands on the surface facilitate the nucleation of cracks [51], thus multiple crack initiation sites are observed. The fatigue striation morphology of the specimens tested at 0.4 % and 0.7 % strain

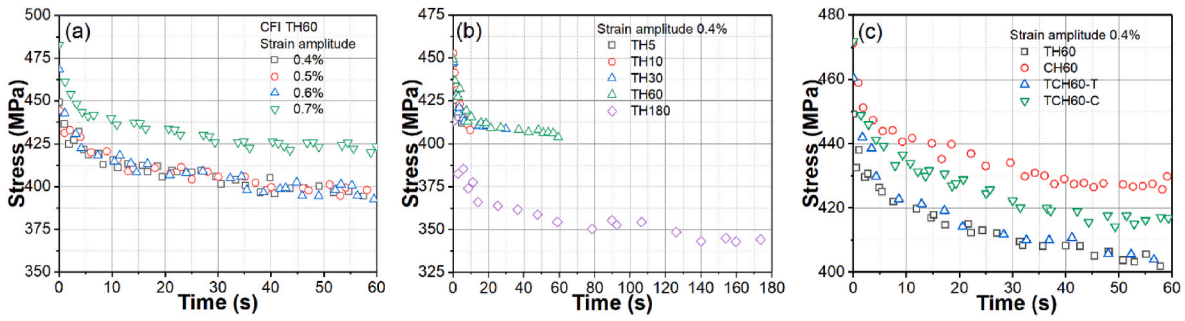

Fig. 9. The evolution of stress with hold time under different loading conditions: (a) tensile hold with different strain amplitudes, (b) tensile hold with different hold times, and (c) different hold directions.

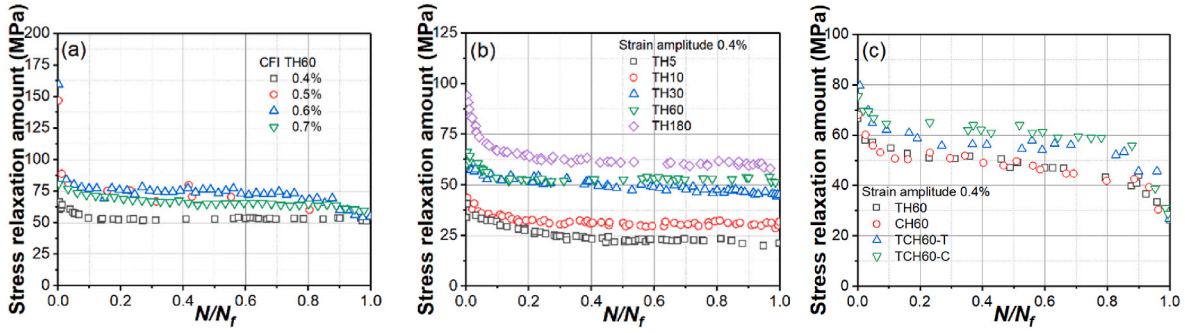

Fig. 10. The evolution of stress relaxation amount: (a) tensile hold at different strain amplitudes, (b) tensile hold with different hold times, and (c) different hold directions.

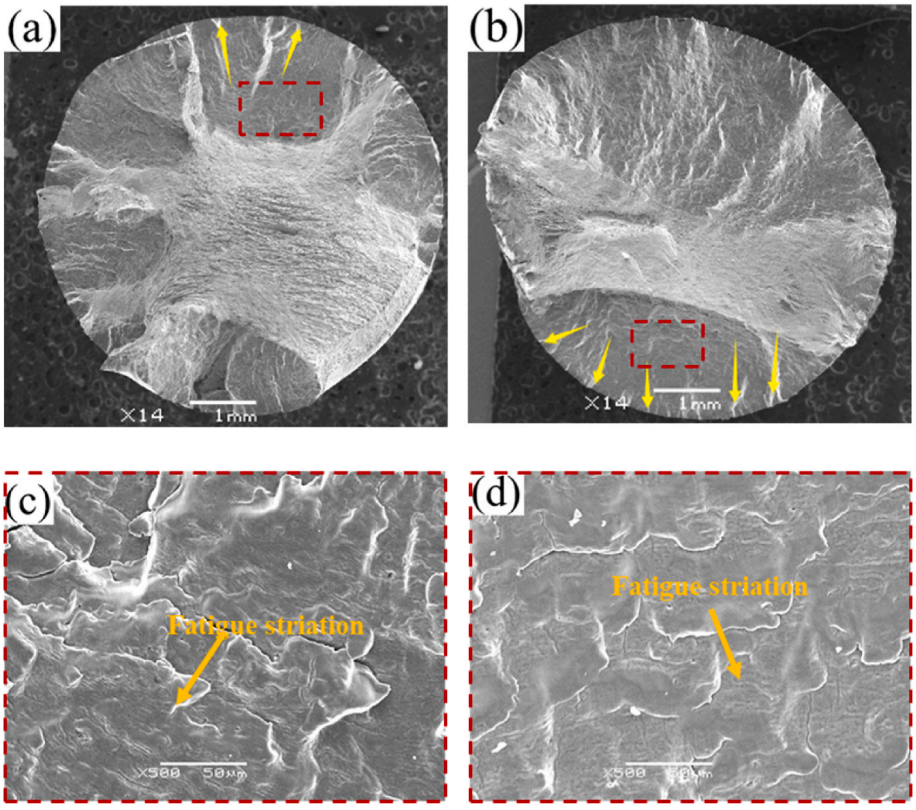

Fig. 11. Fractographs of LCF specimens at different strain amplitudes: (a) and (c) 0.4 %; (b) and (d) 0.7 %.

amplitudes is shown in Fig. 11(c) and (d). These fatigue striations are initially generated by the blunting and sharpening process of cracks caused by dislocation slip in the plastic zone at the fatigue crack tip during cycles [52].

Fig. 12 shows the fractographs of CFI failed specimens with different hold times. Upon introducing the hold time, additional crack initiation sources can be observed (indicated by yellow arrow), as shown in Fig. 12 (b) and (c). This occurrence can be attributed to the surface oxidation of the specimens during long-term CFI tests. Despite the hold time, fatigue striations can still be observed on the fractographs (Fig. 12(e) and (f)). As the hold time increases, the distance between fatigue striations gradually increases. The distance between fatigue striations reflects the crack propagation rate, and an increase in distance indicates an accelerated crack propagation rate [25]. In addition, the common creep void characteristics in the CFI tests only exist in a small amount under tensile hold for 180 s (indicated by green arrow), indicating that the damage mechanism is still fatigue fracture, and an increase in hold time has a significant promoting effect on crack propagation.

Fig. 13 illustrates the fractographs of CFI failed specimens subjected to different hold directions. In comparison to the fractographs obtained during the tensile hold (Fig. 13(a)), the wear during the compressive hold period is relatively severe, resulting in a relatively unclear fractograph. Nevertheless, it is still discernible that numerous crack initiation sites exist in Fig. 13(b) and (c). Fatigue striations are also evident in the fractographs across different hold directions, and a significant number of creep voids are observed in the fractographs of the compressive hold and the combination of tensile and compressive hold. The simultaneous appearance of creep voids and fatigue striations indicates a strong interaction between fatigue and creep, resulting in creep damage that reduces the fatigue life of CFI tests. Among the different hold directions, the combination of tensile and compressive hold (Fig. 13(e)) exhibits the highest number of creep voids, thus indicating its shortest fatigue life.

3.5. Microstructure evolution

Fig. 14 shows the TEM micrographs of the material under various loading conditions. It can be found from Fig. 14(a) that the microstructure of the raw 2.25CrMoV primarily consists of a lath structure. After undergoing cyclic loading (Fig. 14(b)), the lath structure partially recovers, and localized substructure formation occurs with a low dislocation density. However, upon introducing the hold time (Fig. 14(c)), the lath structure undergoes heterogeneous coarsening and exhibits a tendency to transform into a cell structure after a tensile hold for 60 s at a 0.4 % strain amplitude. As the hold time or strain amplitude increases (Fig. 14(d) and (f)), the microstructure undergoes more uniform coarsening, and the lath structure gradually transitions into a homogeneous dislocation cell structure. Similar observations were reported by Fournier et al. [53] in their study on P91 steel, where the martensite lath structure exhibited heterogeneous coarsening at low strain amplitudes and short hold times, while under high strain amplitudes and long hold times, the microstructure displayed uniform coarsening. Zhang et al. [54–56] also observed the interrupted samples of LCF and CFI tests of 9 % Cr steel at high temperature by TEM and found that martensite lath structure gradually evolved into uniform dislocation cell structure, leading to cyclic softening. Fig. 14(e) displays the TEM microstructure of the material subjected to the combination of tensile and compressive hold. In this case, the lath structure transforms into low-energy cell structure with more uniform distribution. This transformation further reduces the resistance to CFI deformation, resulting in dislocation rearrangement. Consequently, cyclic softening and premature failure are observed.

4. Fatigue life prediction

(1) Traditional energy model

Plastic strain energy reflects the energy dissipation during the fatigue process. The use of plastic strain energy density as a damage parameter has been widely used to characterize the LCF behavior of steels at elevated temperatures [57]. The traditional life prediction model based on plastic strain energy is as follows:

$$A\left(\Delta W_p\right)^b = N_f \tag{2}$$

where N_f is the fatigue life, ΔW_p is the plastic strain energy, A and b are material constants. Fig. 15 shows the comparison between the fatigue

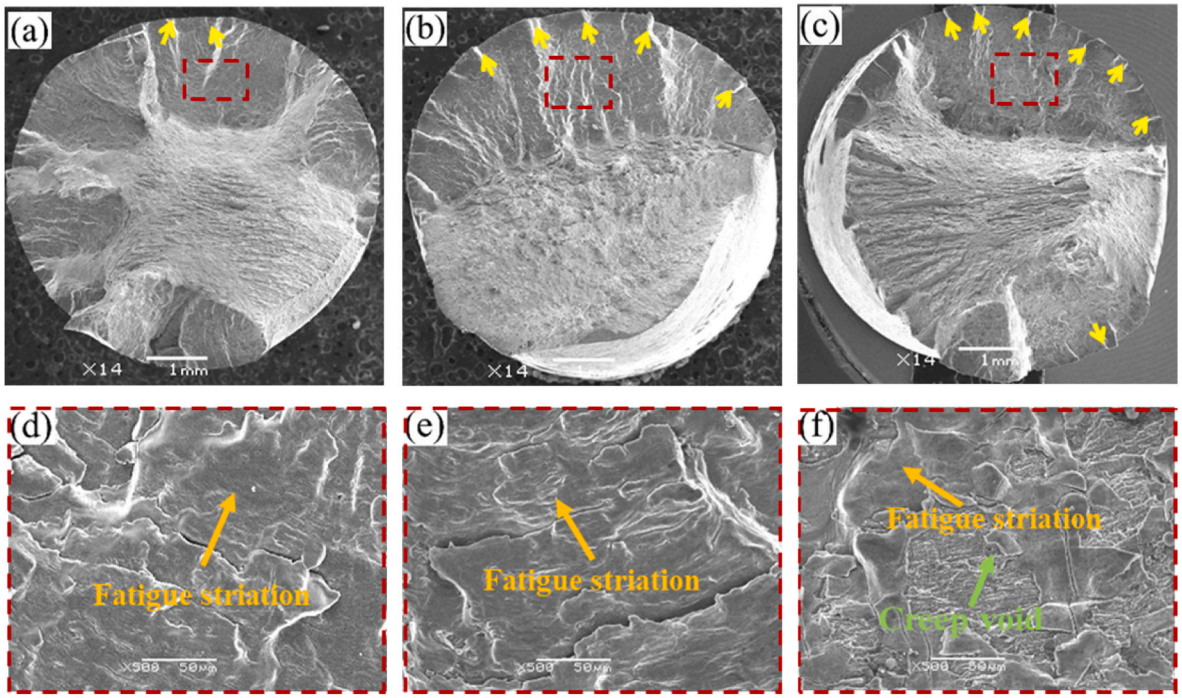

Fig. 12. Fractographs of CFI specimens with different hold times: (a) and (d) 0.4 % TH0; (b) and (e) 0.4 % TH60; (c) and (f) 0.4 % TH180.

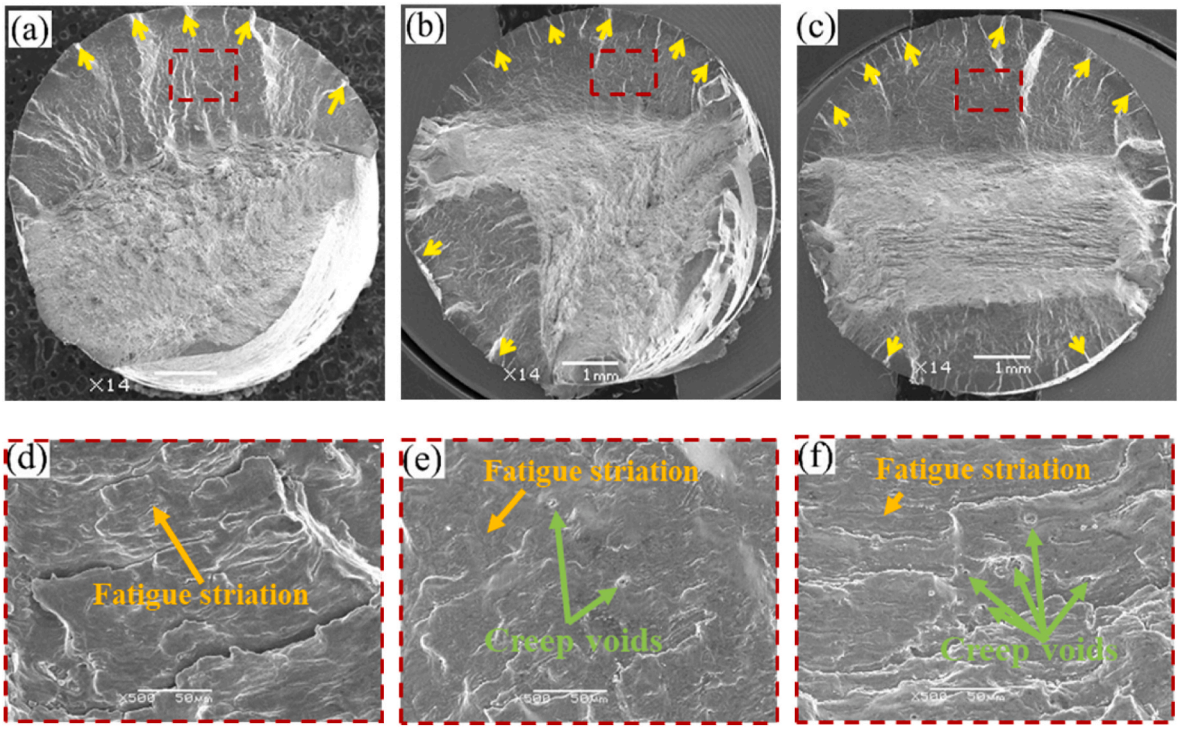

Fig. 13. Fractographs of CFI specimens with different hold directions: (a) and (d) 0.4 % TH60; (b) and (e) 0.4 % CH60; (c) and (f) 0.4 % TCH60.

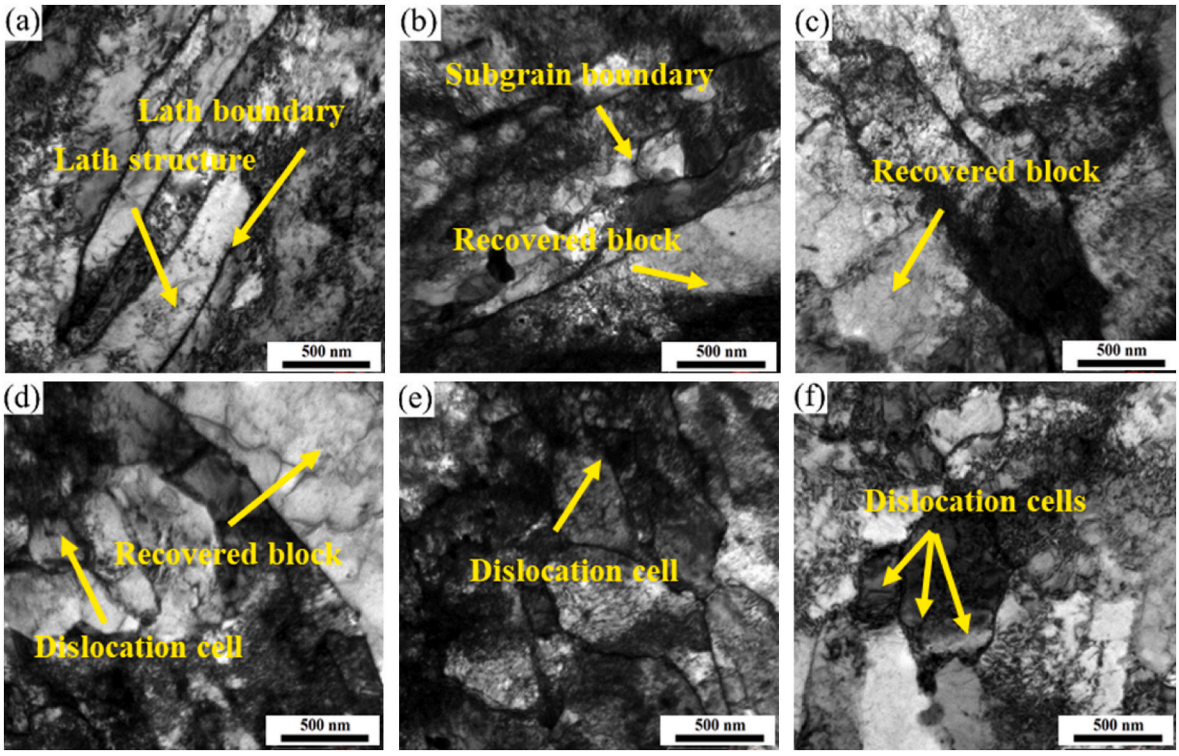

Fig. 14. TEM micrographs of (a) raw material, (b) 0.4 % LCF, (c) 0.4 % TH60, (d) 0.4 % TH180, (e) 0.4 % TCH60, and (f) 0.7 % TH60.

life predicted by the traditional energy model and experimental data, with A = 6408 and b = −1.306. It is obvious that except for a few points, most predictions are within the 1.5 times error. Traditional energy methods have good prediction accuracy for LCF, while life prediction for CFI is generally larger than the experimental life. However, all data points remain within a 2 times error, indicating relatively high prediction accuracy of traditional energy methods.

(2) Modified energy-based model

Due to the fact that traditional energy methods are mostly applicable to the LCF tests for predicting fatigue life, a modified energy-based

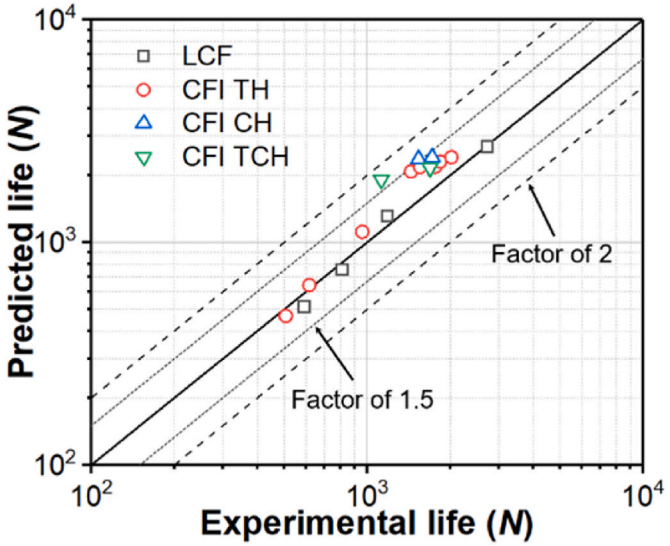

Fig. 15. Comparison of predicted and experimental fatigue life based on the traditional energy model.

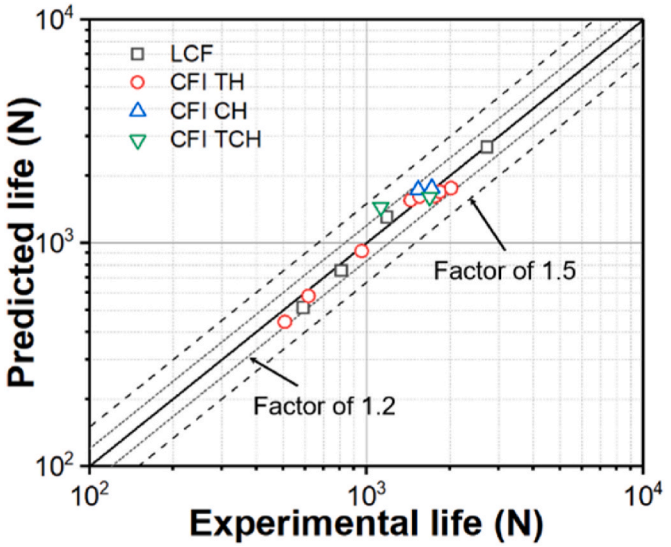

Fig. 16. Comparison of predicted and experimental fatigue life based on the modified energy-based model.

model considering the effect of CFI is necessary. In light of the distinct roles played by tensile and compressive plastic strain energy in CFI tests, the traditional energy method was accordingly modified with the following expression:

$$A\left(\Delta W_{pp}\right)^{b} = N_f \tag{3}$$

$$\Delta W_{pp} = n \bullet \Delta W_{pt} + m \bullet \Delta W_{pc} \tag{4}$$

where N_f is the fatigue life, ΔW_{pp} is the modified plastic strain energy, ΔW_{pt} is the plastic strain energy of tensile section, ΔW_{pc} is the plastic strain energy of compressive section, A and b are material constants, n and m are the contribution values of ΔW_{pt} and ΔW_{pc}, and $n + m = 1$. Fig. 16 displays a comparison between the fatigue life predicted by the modified energy method and experimental data, with $A = 1873$, $b = -1.098$, $n = 0.49$, $m = 0.51$. The results indicate that the majority of predictions fall within a 1.2 times error, showcasing a high level of accuracy in predicting fatigue life. Notably, the modified model also demonstrates good performance in predicting the fatigue life of CFI. When contrasted with traditional energy methods, the modified model exhibits significantly improved prediction accuracy.

5. Conclusion

In this paper, a series LCF and CFI tests were conducted to clarify the deformation behavior, microstructure evolution and fracture behavior of 2.25CrMoV steel at a high temperature of 455 °C. The influences of strain amplitude, hold time and hold direction are elucidated. Through this work following conclusions can be drawn:

(1) 2.25CrMoV steel exhibits significant cyclic softening in both LCF and CFI tests, manifesting three distinct stages: rapid softening, stability, and final failure due to crack initiation and propagation. In LCF tests, the degree of softening increases with higher strain amplitudes, and the introduction of a hold time accelerates the softening process. The combination of tensile and compressive hold results in the lowest fatigue life, followed by compressive hold alone.
(2) Under tensile hold conditions, fatigue fracture remains the predominant failure mode, and longer hold times promote crack propagation. In compressive hold and tensile-compressive hold conditions, an increased presence of creep voids is observed. The interaction between fatigue and creep becomes more pronounced, leading to a reduction in fatigue life.
(3) The lath structure undergoes recovery during cyclic loading, but the introduction of hold time results in uneven coarsening of the lath structure. With longer hold times or higher strain amplitudes, the microstructure transforms into a uniform low-energy dislocation cell structure. This transformation induces dislocation rearrangement, accelerating the process of softening and premature failure.
(4) An improved energy-based model was proposed to predict fatigue life under different loading conditions. Compared to the traditional energy method, the improved model demonstrates higher accuracy in predicting the fatigue life of 2.25CrMoV steel.

CRediT authorship contribution statement

Furen Chen: Methodology, Investigation, Writing – original draft. Wei Zhang: Conceptualization, Supervision, Funding acquisition, Writing – review & editing. Kaihao Zhang: Methodology, Investigation. Qiaofa Yang: Methodology, Investigation, Validation. Xiaoxiao Wang: Investigation, Writing – review & editing. Changyu Zhou: Supervision, Writing – review & editing.

Data availability

Data will be made available on request.

Declaration of competing interest

The authors declare that they have no known competing financial interests or personal relationships that could have appeared to influence the work reported in this paper.

Acknowledgements

The authors gratefully acknowledge the financial support of the National Natural Science Foundation of China (No. 52005250).

References

[1] Rana MS, Sámano V, Ancheyta J, Diaz JAI. A review of recent advances on process technologies for upgrading of heavy oils and residua. Fuel 2007;86:1216–31.

[2] Alshahrani MAM, Ooi SW, Divitini G, Bhadeshia HKDH. Mitigating high temperature hydrogen attack with interphase precipitation. Int J Hydrogen Energy 2023;50:189–98.
[3] Terada S. Code case for extension use of 2.25Cr1Mo0.25V steels for vessels in asme section viii division 3. In: Proceedings of the ASME 2006 pressure vessels and piping, vol. 4756. American Society of Mechanical Engineers; 2006. p. 31–40.
[4] Chaudhuri S, Ghosh RN. Creep behavior of 2.25Cr1Mo steel—effects of thermal ageing and pre-strain. Mater Sci Eng, A 2009;510–511:136–41.
[5] Chu L, Chen X-D, Fan Z-C, Zhou Y, Wu Z-X, Cui Q-F. Characterization of heterogeneous creep deformation in vanadium-modified 2.25Cr1Mo steel weldments by digital image correlation. Mater Sci Eng, A 2021;816:141350.
[6] Peral LB, Amghouz Z, Colombo C, Fernández-Pariente I. Evaluation of hydrogen trapping and diffusion in two cold worked CrMo(V) steel grades by means of the electrochemical hydrogen permeation technique. Theor Appl Fract Mech 2020; 110:102771.
[7] Moro L, Gonzalez G, Brizuela G, Juan A, Simonetti S. Influence of chromium and vanadium in the mechanical resistance of steels. Mater Chem Phys 2008;109: 212–6.
[8] Pillot S, Bourges P, Masson G, Coudreuse L, Toussaint P. Effect of hydrogen on mechanical behavior for 2¼Cr1Mo steel grades (standard and vanadium added). Proceedings of the corrosion. NACE International; 2008.
[9] Zhao Z-Z, Yu D-J, Chen X. Creep-ratcheting-fatigue life prediction of bainitic 2.25Cr1MoV steel. Procedia Struct Integr 2019;17:555–61.
[10] Vantadori S, Carpinteri A, Luciano R, Ronchei C, Scorza D, Zanichelli A. Mean stress effect on fatigue life estimation for Inconel 718 alloy. Int J Fatig 2020;133: 105391.
[11] Szmytka F, Rémy L, Maitournam H, Köster A, Bourgeois M. New flow rules in elasto-viscoplastic constitutive models for spheroidal graphite cast-iron. Int J Plast 2010;26:905–24.
[12] Wang X-X, Chen F-H, Xuan F-Z. Neural network-assisted probabilistic creep-fatigue assessment of hydrogenation reactor with physics-based surrogate model. Int J Pres Ves Pip 2023;206:105051.
[13] Farragher TP, O'Dowd NP, Scully S, Leen B. Thermomechanical analysis of a pressurised pipe under plant conditions. J Pressure Vessel Technol 2013;135: 011204.
[14] Aktaa J, Walter M, Angella G, Perelli Cippo E. Creep-fatigue design rules for cyclic softening steels. Int J Fatig 2019;118:98–103.
[15] Rémy L, Szmytka F, Bucher L. Constitutive models for bcc engineering iron alloys exposed to thermal-mechanical fatigue. Int J Fatig 2013;53:2–14.
[16] Karditsas PJ. Design issues and implications for structural integrity of fusion power plant components. Fusion Eng Des 2009;84:2104–8.
[17] Sakasegawa H, Hirose T, Kohyama A, Katoh Y, Harada T, Asakura K. Microstructural stability of reduced activation ferritic/martensitic steels under high temperature and stress cycling. Fusion Eng Des 2002;61:671–5.
[18] Liang F, Zhang W, Chen F-R, Yin P, Yang Q-F, Chang L, Zhou C-Y. Experimental and constitutive modelling studies of type 316L stainless steel based on internal stress under low cycle fatigue and creep-fatigue interaction. Int J Fatig 2023;175: 107835.
[19] Yin P, Zhang W, Yang Q, Liang F, Zhang G, Xia X, Zhou C. Dynamic strain aging and microstructural damage mechanism of austenitic stainless steel under thermomechanical fatigue in the temperature range of 250–400° C. Int J Fatig 2022;163:107111.
[20] Mohammad KA, Zainudin ES, Salit MS, Zahari I, Ali A. Experimental determination of the fatigue behavior of austenitic 316L stainless steel under fatigue and creep-fatigue tests at high temperature. Int J Metal Steel Res Technol 2013;1:1–11.
[21] Yang Q-F, Zhang W, Guo Y-J, Liang F, Yin P, Chang L, Zhou C-Y. A universal constitutive model considering strain range dependence effect and transient behaviour for both cyclic softening and hardening steels. Eng Fract Mech 2023; 290:109481.
[22] Hecht RL, Weertman JR. The effect of environment on high-temperature hold time fatigue behavior of annealed 2.25 pct Cr 1 pct Mo steel. Metall Mater Trans 1998; 29:2137–45.
[23] Teranishi H, McEvily A. The effect of oxidation on hold time fatigue behavior of 2.25 Cr-1 Mo steel. Metall Trans A 1979;10:1806–8.
[24] Fournier B, Maxime S, Christel C, Michel N, Veronique R, Annick B, Andre P. High temperature creep-fatigue-oxidation interactions in 9-12% Cr martensitic steels. J Nucl Mater 2009;386–388:418–21.
[25] Paul SK, Sivaprasad S, Dhar S, Tarafder S. Cyclic plastic deformation and damage in 304LN stainless steel. Mater Sci Eng 2011;528:4873–82.
[26] Tian Y, Yu D-J, Zhao Z-Z, Chen G, Chen X. Low cycle fatigue and creep-fatigue interaction behaviour of 2.25CrMoV steel at elevated temperature. Mater A T High Temp 2016;33:75–84.
[27] Zahran H, Zinovev A, Terentyev D, Wang X-W, Abdel Wahab M. Experimental investigation and constitutive material modelling of low cycle fatigue of EUROFER97 for fusion applications. J Nucl Mater 2023;588:154809.
[28] Zhao Q, Abdel Wahab M, Ling Y, Liu Z-Y. Fatigue crack propagation across grain boundary of Al-Cu-Mg bicrystal based on crystal plasticity XFEM and cohesive zone model. J Mater Sci Technol 2022;126:275–87.
[29] Zhao Q, Abdel Wahab M, Ling Y, Liu Z-Y. Fatigue crack propagation within Al-Cu-Mg single crystals based on crystal plasticity and XFEM combined with cohesive zone model. Mater Des 2021;210:110015.
[30] Zhang Z, Hu Z-F, Schmauder S, Zhang B-S, Wang Z-Z. Low cycle fatigue properties and microstructure of P92 ferritic-martensitic steel at room temperature and 873 K. Mater Char 2019;157:109923.
[31] Yin P, Zhang W, Guo S, Wen J, Zhang G, Xue F, Zhou C. Thermomechanical fatigue behaviour and damage mechanisms in a 9% Cr steel: effect of strain rate. Mater Sci Eng, A 2021;815:141308.
[32] Zhang W, Zhang X, Zhang K, Liang F, Xia X, Chang L, Zhou C. Multiaxial non-proportional fatigue behaviour and microstructural deformation mechanisms of 9% Cr steel at elevated temperature. Mater Char 2023;203:113158.
[33] Ahiale GK, Choi W-D, Cho S, Park Y-H, Chun Y-B, Oh Y-J. Low-cycle fatigue behavior of reduced activation ferritic-martensitic steel at elevated temperatures. Met Mater Int 2023;29:71–80.
[34] Zhao Z-Z, Chen X. Effect of cyclic softening and stress relaxation on fatigue behavior of 2.25Cr1Mo0.25V steel under strain-controlled fatigue-creep interaction at 728 K. Int J Fatig 2020;140:105848.
[35] Zhang J-F, Yu D-J, Zhao Z-Z, Zhang Z, Chen G, Chen X. Low cycle fatigue of 2.25Cr1Mo steel with tensile and compressed hold loading at elevated temperature. Mater Sci Eng, A 2016;667:251–60.
[36] Goswami T. Low cycle fatigue—dwell effects and damage mechanisms. Int J Fatig 1999;21(1):55–76.
[37] Rho BS, Kim KJ, Nam SW. The effect of hold time and waveform on the high-temperature, low-cycle fatigue properties of a Nb-A286 alloy. Metall Mater Trans 2001;32:2539–46.
[38] Shankar V, Mariappan K, Sandhya R, Laha K, Jayakumar T, Kumar ER. Effect of W and Ta on creep-fatigue interaction behavior of reduced activation ferritic-martensitic (RAFM) steels. Fusion Eng Des 2015;100:314–20.
[39] Fournier B, Sauzay M, Caes C, Noblecourt M, Mottot M, Bougault A, Rabeau V, Pineau A. Creep-fatigue-oxidation interactions in a 9Cr-1Mo martensitic steel. Part I: effect of tensile holding period on fatigue lifetime. Int J Fatig 2008;30:649–62.
[40] Chen G, Zhang Y, Xu DK, Lin YC, Chen X. Low cycle fatigue and creep-fatigue interaction behavior of nickel-base superalloy GH4169 at elevated temperature of 650°C. Mater Sci Eng, A 2016;655:175–82.
[41] Parker J. Creep fatigue interactions in power plant components. Mater A T High Temp 2014;31:370–7.
[42] Fournier B, Dalle F, Sauzay M, Longour L, Salvi M, Caës C, Tournié I, Giroux P-F, Kim S-H. Comparison of various 9-12% Cr steels under fatigue and creep-fatigue loadings at high temperature. Mater Sci Eng, A 2011;528:6934–45.
[43] Lee SY, Lu YL, Liaw PK, Chen LJ, Thompson SA, Blust JW, Browning PF, Bhattacharya AK, Aurrecoechea JM, Klarstrom DL. Tensile-hold low-cycle-fatigue properties of solid-solution-strengthened superalloys at elevated temperatures. Mater Sci Eng, A 2009;504:64–72.
[44] Ozkan F, Aktaa J. Creep fatigue assessment for EUROFER components. Fusion Eng Des 2015;100:536–40.
[45] Kim K-C, Ma Y-W, Kong B-O, Kim M-S, Kang S-T. Effect of strain rate on low cycle fatigue with hold time in 9Cr rotor steel. Mater Res Innovat 2013;17:332–6.
[46] ASTM E606-04. Standard practice for strain-controlled fatigue testing. West Conshohocken, PA: ASTM International; 2004.
[47] Wang X-W, Gong J-M, Zhao Y-P, Wang Y-F, Yu M-H. Characterization of low cycle fatigue performance of new ferritic P92 steel at high temperature: effect of strain amplitude. Steel Res Int 2015;86:1046–55.
[48] Wang X-W, Zhang W, Gong J-M, Abdel Wahab M. Low cycle fatigue and creep fatigue interaction behavior of 9Cr-0.5Mo1.8W-V-Nb heat-resistant steel at high temperature. J Nucl Mater 2018;505:73–84.
[49] Ye D, Matsuoka S, Nagashima N, Suzuki N. The low cycle fatigue, deformation and final fracture behavior of an austenitic stainless steel. Mater Sci Eng, A 2006;415: 104–17.
[50] Shankar V, Sandhya R, Mathew MD. Creep-fatigue-oxidation interaction in Grade 91 steel weld joints for high temperature applications. Mater Sci Eng, A 2011;528: 8428–37.
[51] Li B-B, Zheng Y, Shi S, Liu Y-M, Li Y-J, Chen X. Microcrack initiation mechanisms of 316LN austenitic stainless steel under in-phase thermomechanical fatigue loading. Mater Sci Eng, A 2019;752:1–14.
[52] Zhang J-G, Chen X, Li Z, Tian F-Z, Liu X-L. Low-cycle fatigue performance and fracture mechanism of nickel-based single crystal superalloy at 530 °C. Rare Met Mater Eng 2023;52(6):8–12.
[53] Fournier B, Maxime S, Alexandra R, Françoise B, André P. Microstructural evolutions and cyclic softening of 9%Cr martensitic steels. J Nucl Mater 2009; 386–388:71–4.
[54] Zhang W, Wang X, Gong J, Jiang Y, Huang X. Experimental and simulated characterization of creep behavior of P92 steel with prior cyclic loading damage. J Mater Sci Technol 2017;33(12):1540–8.
[55] Zhang W, Wang X, Li X, Gong J, Wahab MA. Influence of prior low cycle fatigue on microstructure evolution and subsequent creep behavior. Int J Fatig 2018;109: 114–25.
[56] Zhang W, Wang X, Chen H, Zhang T, Gong J. Evaluation of the effect of various prior creep-fatigue interaction damages on subsequent tensile and creep properties of 9% Cr steel. Int J Fatig 2019;125:440–53.
[57] Ostergren WJ. A damage function and associated failure equations for predicting hold time and frequency effects in elevated temperature, low cycle fatigue. J Test Eval 1976;4(5):327–39.